Electron Delocalization in the Metallabenzenes: A Computational Analysis of Ring Currents

Ganga Periyasamy,[†] Neil A. Burton,*[,†] Ian H. Hillier,[†] and Jens M. H. Thomas[‡]

School of Chemistry, University of Manchester, Manchester, M13 9PL, U.K., and STFC Daresbury Laboratory, Warrington, WA4 4AD, U.K.

Received: November 5, 2007; Revised Manuscript Received: March 20, 2008

Many metallabenzene complexes appear to exhibit an enhanced thermodynamic stability which has been attributed to the concept of aromaticity. Analysis of the ring currents induced by a magnetic field, either by direct visualization or by considering nuclear or nucleus-independent chemical shielding values (NMR or NICS), have become useful theoretical tools to characterize the aromaticity of many molecules involving the main group elements. We have analyzed 21 metallabenzenes using variations of these techniques, which take account of the large core and metal orbital contributions which often lead to transition-metal-containing systems exhibiting anomalous shielding values. Analysis of individual orbital contributions to both the ring currents and chemical shielding values based upon the ipsocentric and CSGT (continuous set of gauge transformations) methods has shown that complexes such as the 18 electron Ir or $Rh(C_5H_5)(PH_3)_2Cl_2$ molecules should be classed as aromatic, whereas the 16 electron complexes such as Os or $Ru(C_5H_5)(PH_3)_2Cl_2$ should not, despite having the same occupancy of π-MOs. The differences can be directly attributed to the HOMO/LUMO b_2 in-plane (d_{xy}) molecular orbital, which, when unoccupied, is available to disrupt the delocalized currents typical of aromatic systems. A range of Pd and Pt metallabenzenes with cyclopentadienyl and phosphine ligands is also discussed as having aromatic and nonaromatic character, respectively.

Introduction

The ring current model (RCM)[1] was proposed 60 years ago and is still widely used to rationalize the magnetic properties of aromatic molecules and as a criterion for determining the aromaticity of cyclic molecules. Although the aromaticity of a wide range of systems, particularly unsaturated organic molecules, has been exhaustively studied,[2] this aspect of bonding in transition-metal complexes has been considerably less well characterized. In particular, the electronic structure and thermodynamic stability of metallabenzenes, which are metallacyclic benzenoid compounds in which the CH group of benzene has been replaced by a transition metal and its associated ligands, have been the subject of some discussion in recent years.[3] However, in contrast to cyclic organic molecules, the use of the RCM and criteria based upon the magnetic response of these molecules to determine aromaticity, such as the NMR chemical shielding of ring protons, are complicated by the strong local (diamagnetic) current circulations induced around or by the metal atoms. In this paper, we have studied a range of metallabenzene complexes, containing Ir, Rh, Os, Ru, Pt, and Pd, using computational approaches to explore the ring current circulations in order to discuss the degree of aromaticity (nonaromaticity or antiaromaticity) and to provide an explanation based directly upon the molecular orbital occupancies.

The essential features of the RCM were initially outlined by Pauling,[4] Lonsdale,[5] and London[6] (PLL) in an attempt to explain the experimental magnetic susceptibility and the proton NMR chemical shift of benzene. In these seminal papers, they conclude that "the susceptibility ellipsoids of aromatic molecules are found to be approximately prolate ellipsoids of revolution, with the long axis normal to the plane of the ring system"[1] and that "the diamagnetic susceptibility of aromatic molecules is numerically much greater in a direction normal to the plane of the molecule than in the directions parallel to the molecular plane".[4,6] The diamagnetic ring current induced by the magnetic field perpendicular to the molecular plane was shown[7,8] to directly contribute to the peculiar downfield chemical shift of the ring protons.[9,10] This enhancement of magnetic susceptibility and magnetic anisotropy observed experimentally for benzene was thus ascribed to the special mobility of delocalized π-electrons and provided the first evidence for the concept of ring currents. Similar downfield chemical shifts were observed in other organic molecules like 1,4-polymethylenebenzenes,[11] annulenes, especially in bridged annulenes, together with their protonated cations, dications (2e oxidation), and dianions (2e reduction), which have since been used as important probes of aromaticity and as a means to test experimentally the Huckel rule.[12] There are many other examples where diamagnetic currents are not restricted to individual atoms, such as in bismuth, antimony, graphite, and condensed aromatic ring systems.[13–19] Although many earlier investigations of aromaticity were formulated with Huckel molecular orbital theory (HMO),[20–23] it is now common to use ab initio Hartree−Fock or density functional theory to interpret the magnetic properties and the NMR spectra of unsaturated and aromatic molecules.[24,25] Early use of the PLL model, and its reformulations by Pople[26] and McWeeny,[27] was also used to obtain numerical estimates of chemical shift arising directly from ring currents.[28–33]

An important aspect of magnetic susceptibility and nuclear magnetic shielding is that they can theoretically be expressed as sums of diamagnetic (diatropic)[11] and paramagnetic (paratropic)[34,35] current contributions. Recently, these concepts have been further explored by Steiner and Fowler,[36] who have qualitatively related the diatropic and paratropic contributions to specific molecular orbitals, thus allowing the determination

* To whom correspondence should be addressed. E-mail: neil.burton@manchester.ac.uk.
[†] University of Manchester.
[‡] STFC Daresbury Laboratory.

10.1021/jp7106044 CCC: $40.75
Published on Web 06/11/2008

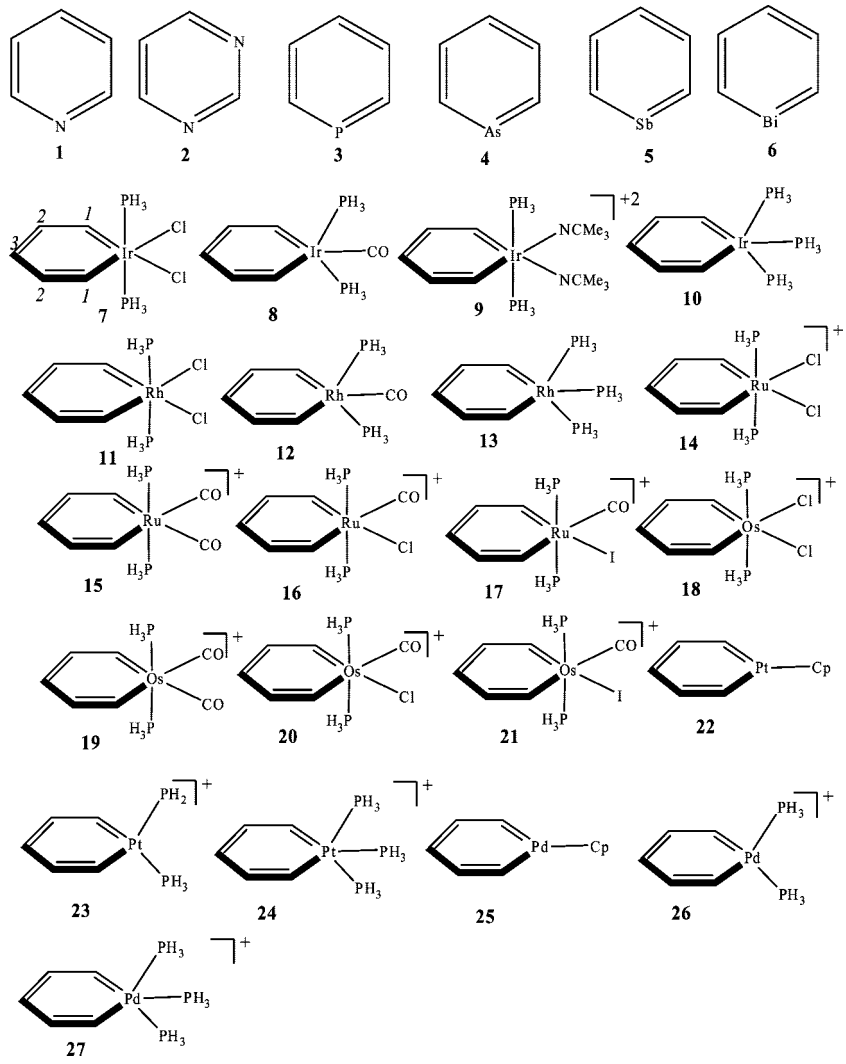

Figure 1. Definitions of the hetero- and metallabenzene complexes.

of which electrons in a conjugated system are explicitly responsible for the ring currents. For example, for molecules with a single ring and $(4n + 2)$ π-electrons, they have shown that exactly four of the electrons are responsible for the induced diatropic current, whereas just two electrons are responsible for the induced paratropic current (indicative of antiaromaticity) in $4n$ electron systems.[37] Using the ipsocentric distributed gauge-origin formulation,[38] induced current density vector field plots[25] can be generated that are independent of any origin or reference point so that the ring current circulations can also be directly visualized. By partitioning these quantities, either the induced current density or the chemical shielding, into contributions from individual molecular orbitals, the local contribution of lone pairs and σ-bonds to the total chemical shielding and to the total ring current can also be eliminated.[36] Thus, the individual contributions of the remaining delocalized π-electron circulation can be categorized as either aromatic, with a diatropic circulation around the ring, nonaromatic, with localized or broken circulation, or antiaromatic, which corresponds to a paratropic circulation.

Magnetic shielding properties, particularly proton NMR chemical shifts or magnetic susceptibility, have been widely used as quantitative experimental measures of the aromatic character of a molecule, and these quantities can be reproduced using computational methods. However, chemical shielding does not only depend purely on the π-electron system but also on the combination of other magnetic shielding contributions due to local circulations of electrons in bonds, lone pairs, and the atomic cores.[39,40] As a result, downfield isotropic chemical shifts have not, in general, proved to be a reliable measure of aromaticity,[41] and, for example, the proton chemical shift values of aromatic benzene, furan, and pyrole molecules only differ from the antiaromatic cyclopentadiene molecule by a few parts per million.

Computationally, there are a number of other ways in which the degree of aromaticity can be quantified, although perhaps, the most common are those based upon the nucleus-independent chemical shift (NICS), originally proposed by Schleyer et al.[2] In these approaches, the chemical shielding value is computed at the center of a ring, NICS(0), or at points above the ring to minimize the contribution of the σ-electrons; for example, the NICS(1) value is computed at 1 bohr above the ring center of the plane of the ring. A particular drawback of these approaches is that the methods do not provide an absolute measure and rely, to a large extent, on the values obtained from similar reference molecules that are known to be aromatic, such as benzene, so that there is no natural reference point for a linearly, branched, or even 3D-conjugated or organometallic system.[40,42] In addition, earlier studies by Schleyer et al.[39] note that magnetic criteria such as NICS,[43] magnetic susceptibility, and isotropic ^{1}H chemical shielding may be severely limited for systems such as the metallabenzenes due to the large σ-current at the metal center. We shall show that this is indeed the case but that these

effects can be discounted if only the out-of-plane molecular orbital contributions are considered.

The main focus of this paper is to study and understand the aromatic character of a range of heterobenzenes and metallabenzenes. Six heterobenzenes (**1**−**6**; Figure 1) are initially considered since they are useful as reference compounds and to validate the approach which will be used to study the metallabenzenes. We shall then consider a number of 18 electron (**7**−**13**; Figure 1) and 16 electron (**14**−**21**; Figure 1) metallabenzenes that have previously been studied using both experimental and theoretical methods that have employed a range of other criteria to categorize them as either aromatic or nonaromatic. In each of these cases, the metallabenzenes have 10 π-electrons, and according to the Huckel $(4n + 2)$ π-electron rule, they could all be aromatic[44] Furthermore, some metallabenzenes, especially iridabenzenes **9** and **10**, have reactivity which contradicts that expected of normal aromatic molecules by easily undergoing cycloaddition, cyclopentadienyl formation, or a range of substitution reactions.[45–48] On the basis of these reactivity criteria, and particularly that they easily undergo addition reactions, some of these metallabenzenes have been suggested not to be aromatic. On the other hand, the delocalized molecular orbitals are very similar to benzene,[49] and the stabilization energies obtained by extensive energy decomposition analyses (EDA)[2,50,51] for all of the molecules suggest that they should all be classified as aromatic after all. Further evidence for aromatic character can be found in that each molecule is planar and that nearly all of the ring protons exhibit a downfield ^{1}H NMR chemical shift (below 7 ppm).[44–46] Since the previous analyses of these systems suggest different conclusions, a different approach is used here using a magnetic criterion to determine the aromaticity of these complexes. Our analysis will be based upon the detailed analysis of the ring currents and chemical shielding values which discount the contributions of the metal σ-orbitals that would otherwise obscure reliable interpretation. In particular, we shall employ the NICS(1) approach, including only the out-of-plane (π) molecular orbitals, as a quantitative measure of the magnetically induced π-electron density in the complexes along with a detailed analysis of the differences in each molecular orbital contribution to the π-ring currents of the 16e and 18e complexes to understand the origin of the aromaticity/antiaromaticity. In the final section, we shall also present an analysis of three recently synthesized[45] platinum− (**22**−**24**; Figure 1), and three palladium−metallabenzenes (**25**−**27**; Figure 1).

Theoretical Background

Induced current density tensors can be readily and accurately calculated at many points in a molecular system using the distributed-origin ipsocentric approach.[25,36] The benefits of this method, also known as the CTOCD-DZ (continuous transformation of origin of current density-diamagnetic zero) formulation of coupled Hartree−Fock theory,[52] is that the current density at each point is calculated with the gauge origin at that point. A direct consequence of choosing the gauge origin to be coincident with each point is that there is no diamagnetic contribution to the current density at each point; although by considering rotational angular momentum about a global center of coordinates, rather than about each point, both diatropic and paratropic currents will be observed overall, particularly around nuclei, bonds, and rings.

For a closed-shell molecule with N electrons, the total first-order induced current density at point $\mathbf{r}$ is

$$\mathbf{j}^{(1)}(\mathbf{r}) = \frac{ie\hbar N}{m_e}\left[\int \left(\Psi_0 \nabla \Psi_0^{(1)} - \Psi_0^{(1)} \nabla \Psi_0\right) d\tau\right] \quad (1)$$

where Ψ_0 is the unperturbed wave function, and the first-order magnetically perturbed wave function $\Psi_0^{(1)}$ is given by

$$\Psi_0^{(1)} = \frac{e}{2m_e}\left[\sum_{I>0} \Psi_I \frac{\langle \Psi_I | \hat{\mathbf{L}}(\mathbf{0}) | \Psi_0 \rangle}{E_I - E_0}\right] \cdot \mathbf{B} + \frac{e}{2m_e}\left[\mathbf{r} \times \sum_{I>0} \Psi_I \frac{\langle \Psi_I | \hat{\mathbf{P}} | \Psi_0 \rangle}{E_I - E_0}\right] \cdot \mathbf{B} \quad (2)$$

$$= \Psi_0^{(p)} + \Psi_0^{(d)}$$

In this equation, $\hat{\mathbf{L}}(\mathbf{0})$ is the angular momentum operator for rotation about a global origin of coordinates, and $\hat{\mathbf{P}}$ is the translational angular momentum operator. For a symmetric molecule, it has been shown that consideration of the perturbed wave function in this form allows us to simplify our understanding of which excitations will contribute to the total current density; allowed excitations from occupied to virtual molecular orbitals via the translational operator will give rise to a diatropic term ($\Psi_0^{(d)}$), and those via the rotation operator will give rise to a paratropic term ($\Psi_0^{(p)}$).

It is also important that in this formulation, $\mathbf{j}^{(1)}$ can be written as a sum of occupied molecular orbital dependent terms

$$\mathbf{j}^{(1)}(\mathbf{r}) = 2\sum_{n=1}^{N/2} \mathbf{j}_n^{(1)}(\mathbf{r}) \quad (3)$$

where $\mathbf{j}_n^{(1)}$ is the first-order induced current density for molecular orbital n and the summation is over $N/2$ molecular orbitals. In this way, the total current density for each molecular orbital, or groups of orbitals such as the out-of-plane (π) orbitals only, can be studied.[53] We shall subsequently see that there are large contributions to $\mathbf{j}^{(1)}$ from the large numbers of electrons in the atomic cores or the occupied metal orbitals. These tend to dominate the magnetic properties and are also difficult to visualize.[40] A clearer picture of the metal−ligand (M−L) bonding will be obtained by eliminating the $\mathbf{j}_n^{(1)}$ associated with these orbitals from the total expansion or by considering the orbitals separately.

Either total or induced current density vectors for specific orbitals, indicating the magnitude and direction of the induced current density at each point in a given magnetic field, can be obtained directly from the corresponding tensor. It is often convenient to define a molecular plane and project onto it the current density vectors due to a uniform external magnetic field, $\mathbf{B}$, defined perpendicular to it. We shall adopt the usual convention considering the magnetic field to be directed into the plane; in this case, we shall choose planes parallel to the ring of the metal and ligand atoms such that an anticlockwise diatropic ring current circulation is associated with delocalization and aromaticity and a clockwise paratropic ring current is associated with antiaromaticity.

Although the actual computation of the $\mathbf{j}^{(1)}$ in the ipsocentric method is made by a coupled Hartree−Fock or Kohn−Sham procedure, and therefore includes self-consistent terms, the perturbation expansion can be used to rationalize the computed current density maps. Fowler and Steiner have shown that in symmetric molecules, such as benzene, it is possible to use them to understand the various contributions to $\mathbf{j}^{(1)}$ by application of simple group theory. Here, we shall exploit the high symmetry of the metallabenzene transition-metal complexes to distinguish the allowed transitions which would contribute to the expansion

of $\mathbf{j}^{(1)}$ and therefore understand the origin of the various observed current circulations.

Since $\hat{\mathbf{L}}$ and $\hat{\mathbf{P}}$ can be expressed as sums of one-electron operators, $\hat{\mathbf{l}}$ and $\hat{\mathbf{p}}$, eq 2 may be expanded in terms of the occupied (ψ_n) and unoccupied (ψ_p) MOs and their orbital energies, ε_i.

$$\psi_n^{(1)}(\mathbf{r}) = -\frac{e}{2m_e}\left[\sum_{p>N/2} \psi_p(\mathbf{r})\frac{\langle\psi_p|\hat{\mathbf{l}}(\mathbf{0})|\psi_n\rangle}{\varepsilon_p - \varepsilon_n}\right]\cdot\mathbf{B} + \frac{e}{2m_e}\left[\mathbf{r}\times\sum_{p>N/2} \psi_p(\mathbf{r})\frac{\langle\psi_p|\hat{\mathbf{p}}|\psi_n\rangle}{\varepsilon_p - \varepsilon_n}\right]\cdot\mathbf{B} \quad (4)$$

Following Steiner and Fowler,[36] if $\Gamma(\psi_n)$, $\Gamma(\psi_p)$, $\Gamma(\mathrm{R})$, and $\Gamma(\mathrm{T}_\perp)$ are the representations of the occupied and unoccupied MOs, rotation about the magnetic field direction, and translation perpendicular to the field direction, respectively, then if $\Gamma(\psi_n) \times \Gamma(\psi_p) \times \Gamma(\mathrm{R})$ contains Γ_0, the totally symmetric representation, the transition will be allowed, and there would be a paramagnetic contribution. Similarly, if $\Gamma(\psi_n) \times \Gamma(\psi_p) \times \Gamma(\mathrm{T}_\perp)$ contains Γ_0, then there would be a diamagnetic contribution to $\mathbf{j}_n^{(1)}$. It is useful to bear in mind that the most dominant transitions will usually be those between the orbitals near the Fermi level, and this will be reflected in the O-NICS and O-NMR values, which we shall discuss next.

Next, we shall turn our attention to integrated magnetic properties and, in particular, to the nuclear magnetic (chemical) shielding tensor. In this work, we shall mainly consider the CSGT (continuous set of gauge transformations) method[25] for computing the chemical shielding since this approach closely follows the ipsocentric formulation discussed above, and similar orbital and symmetry considerations will apply. In the CSGT method, the shielding tensor can be given by

$$\sigma_{\alpha\beta}^N = \frac{\partial^2 E}{\partial B_\beta\, \partial m_{N_\alpha}} = -\frac{1}{Bc}\int\left(\frac{\mathbf{r}_N\times\mathbf{j}_\beta^{(1)}(\mathbf{r})}{r_N^3}\right)_\alpha \mathrm{d}\mathbf{r}_N \quad (5)$$

where m_N is the nuclear magnetic moment, and a gauge transformation is performed at each integration point when calculating the total current density vector $\mathbf{j}(\mathbf{r})$. The shielding tensor, $\boldsymbol{\sigma}^N$, can be partitioned into a sum of molecular orbital terms, $\boldsymbol{\sigma}_n^N$, each defined in terms of the orbital current density, $\mathbf{j}_n(\mathbf{r})$

$$\boldsymbol{\sigma}^N = 2\sum_{n=1}^{N/2} \boldsymbol{\sigma}_n^N \quad (6)$$

This approach, resulting in $N/2$ independent isotropic chemical shielding values for each nucleus, will be referred to by the O-NMR (orbital-NMR) acronym. When the shielding is computed at a non-nuclear center, such as at the center of a ring, the shielding values derived from specific molecular orbitals will be referred to by the O-NICS acronym,[50] analogous to conventional (isotropic) NICS values which are computed using the total current density. Similar schemes, such as the dissected NICS method, have been previously proposed and partition NICS values within the GIAO (gauge including atomic orbital) scheme.[50] Although conventional isotropic NICS indices, such as NICS(1), correlate well with aromatic stabilization energies for organic molecules, particularly when only the contribution from the π-orbital density is considered, recent studies[54] have shown that a nonisotropic index, based only on shielding tensor components perpendicular to the ring plane, NICS(0)$_{\pi zz}$,[53] or the simpler NICS(1)$_{zz}$ index, are particularly reliable measures of aromatic stabilization. In this study, as our most reliable indicator of aromaticity, we preferred to employ an isotropic index which reflects the ring current above the ring plane but which also neglects the core and σ-electrons, O$_\pi$-NICS(1); this approach was found to consistently give similar relative indices, with the same sign although smaller in magnitude, to NICS(1)$_{zz}$ or O$_\pi$-NICS(1)$_{zz}$ indices for all of the complexes studied here. There has been considerable debate in the literature in the past regarding the most appropriate way to compute nuclear chemical shielding, and we recognize that the GIAO scheme, which uses gauge including atomic basis functions, is widely regarded as the most accurate when a large basis set is used; however, it is also appropriate to note that chemical shifts and relative isotropic shielding values are well reproduced by both the GIAO and the CSGT methods, as we shall later show for the metallabenzene complexes.

Finally, we shall consider the anisotropy of the induced current density (ACID), $\Delta T_S^{(1)}$ as proposed by Herges et al.,[40] which can also be computed from the current density tensor at each point

$$\Delta T_S^{(1)}(\mathbf{r})^2 = \frac{1}{3}[(\mathbf{j}_{xx} - \mathbf{j}_{yy})^2 + (\mathbf{j}_{yy} - \mathbf{j}_{zz})^2 + (\mathbf{j}_{zz} - \mathbf{j}_{xx})^2] + \frac{1}{2}[(\mathbf{j}_{xy} + \mathbf{j}_{yx})^2 + (\mathbf{j}_{xz} + \mathbf{j}_{zx})^2 + (\mathbf{j}_{yz} + \mathbf{j}_{zy})^2] \quad (7)$$

The ACID is an alternative to the direct use of the current density; it is a scalar dimensionless quantity which is independent of the direction and magnitude of the magnetic field and which can be used as an indication of the degree of electron delocalization in a molecule. Similar to the usual interpretation in conjunction with 3D isosurfaces of equivalent ACID values, 2D contours plotted in or above the plane of the molecular ring delimit regions of similar density of delocalized electrons. Being linearly independent of the total electron density and only considering the anisotropy of the interatomic currents, the analysis should also not be encumbered with the same limitations of being overwhelmed by large currents due to in-plane or core orbitals.

Computational Details

All of the complexes discussed in this paper (see Figure 1) were optimized using the B3LYP hybrid density functional[55] with the 6-31+G(d) basis set for hydrogen, carbon, nitrogen, oxygen, phosphorus, sulfur, chlorine, and arsenic. The LANL2DZ[56] atomic pseudopotential and basis set were used for bismuth, antimony, iodine, ruthenium, iridium, rhodium, osmium, platinum, and palladium. Although we do not discuss the optimized geometries of the compounds because the focus of this work lies on the magnetic properties of the metallabenzenes, the calculated bond lengths and bond angles are comparable in each case with experimental values.

All electronic structure calculations were performed using the Gaussian 03 program,[57] which was modified by us to compute the O-NICS, O-NMR, and the ipsocentric induced current density vectors at each point based upon the original implementation of the CSGT method.[25] The implementation was verified against previously published data for benzene, cyclopentadiene, pyrole, and furan molecules.[53,58] The current density plots were rendered by the CCP1-GUI program,[59] enabling both streamline and contour plots that are not overwhelmed by the relatively high values of the core and metal orbital current densities. On the plots, the contours or streamlines represent either the relative magnitude of the current density, $|\mathbf{j}|$, or the ACID values, and the arrows represent the direction of the induced current density vectors projected onto the plotting plane.

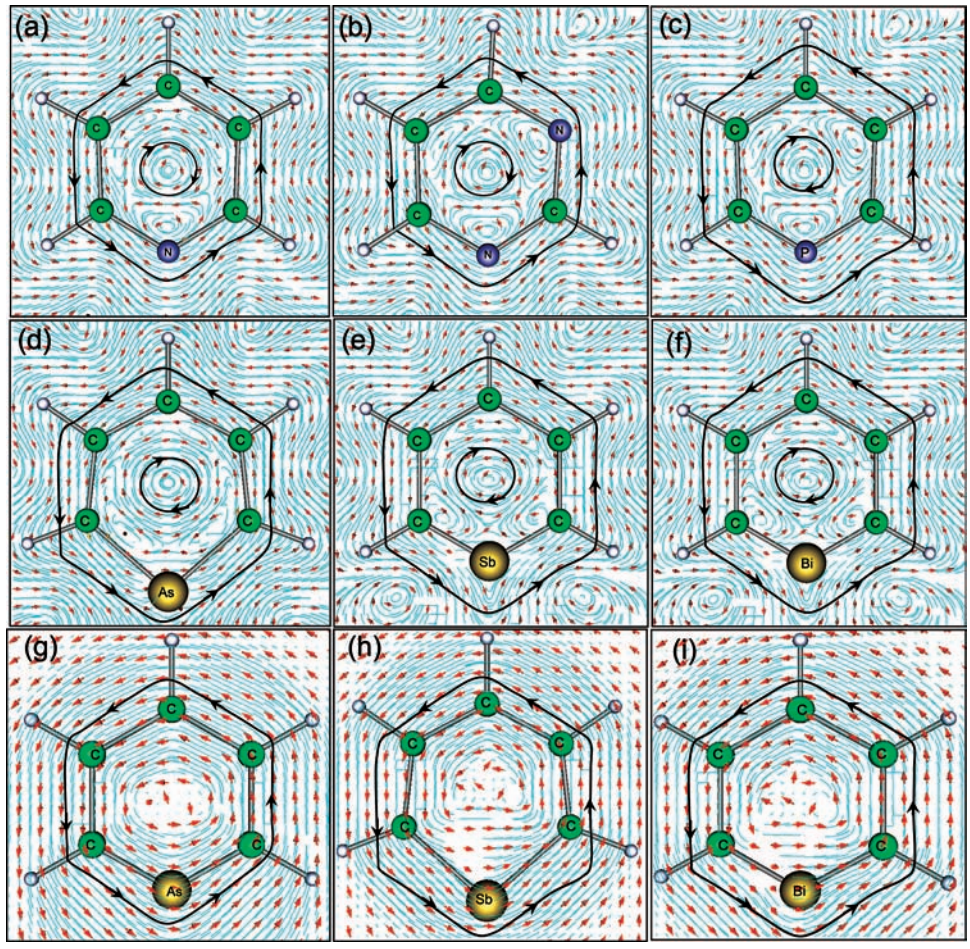

Figure 2. Total induced current density plots at 1 bohr above the ring plane for complexes (a) **1**, (b) **2**, (c) **3**, (d) **4**, (e) **5**, and (f) **6**. Induced current density for the out-of-plane molecular orbitals at 1 bohr above the ring plane for complexes (g) **4**, (h) **5**, and (i) **6**.

In some cases, the global ring current is also indicated by hand drawn annotations for clarity. Although the magnitude of the current density vectors can be directly rendered on some orbital plots by scaling the arrows (either by length or area),[53] such representations have not proved to be particularly visually informative for the metallabenzenes due to the large relative magnitudes of the current density involved. Instead, to gauge the relative magnitudes of the currents of each orbital, we shall compare an O-NICS(1) index, and for the complexes, we shall compare O_π-NICS(1) indices based upon the current density of the valence out-of-plane MOs. For the NICS(0) and NICS(1) calculations, the ring centers were taken to be at the ring critical points.[52]

Ring Current Analyses of the Heterobenzenes

The replacement of the CH group in benzene by group-15 elements results in the heterobenzenes, which are useful as reference compounds to compare with the chemistry of the metallabenzenes. Previous computational studies employed an EDA and concluded that the heterobenzenes are more aromatic than benzene.[51] The substitution of carbon in benzene **1** by nitrogen or phosphorus (**2** and **3**, respectively) increases the number of electrons in the six-membered ring from six to seven. Figure 2a−f, which contains plots of the total current density in a plane 1 bohr above the ring for the six complexes, in each case, clearly shows a diatropic ring current above the nuclei of the ring atoms similar to that of the π-system of benzene. A local circulation is evident near to the heteroatom due to the lone pair orbital. The inclusion of heavier elements like As (**4**), Sb (**5**), and Bi (**6**) further distorts the ring current by creating a strong local circulation at the heteroatomic center due to the core electrons. This feature is less evident when the induced current density for only the three occupied valence π-orbitals is plotted for **4**−**6**, and Figure 2g−i shows a similar circulation to three out-of-plane occupied molecular orbitals of benzene and complexes **1**−**3**. All of the heterobenzene complexes clearly have the features typical of aromatic systems, a paratropic current inside of the ring and an outer diatropic current around the ring due to delocalization of the π-electrons, even though they do not follow the Huckel $(4n + 2)$ π-electron rule.

To quantify these observations, the O_π-NICS(1) values and the O_π-NMR chemical shielding values for ^{13}C and the ring protons of these complexes were computed and are presented in Table 1. For all six heterobenzene molecules, the O_π-NICS values are negative, which is a clear indication of aromatic delocalization and agrees with the conclusions of earlier EDA and total NICS analysis. Although the total shielding values are difficult to compare due to the different atomic cores, the negative O_π-NICS values for the π-MOs of the complexes are similar, although complex **1**, with a value of −20.4 ppm, does appear to exhibit slightly greater aromatic character than the other complexes **2**−**6**, which have values ranging from −17.4 to −18.5 ppm. The analysis does show that at 1 bohr above the plane, the total NICS values down the group are relatively similar to those involving only the π-orbitals, as we might expect, although the total NMR isotropic shielding values are

TABLE 1: Total and π-Molecular Orbital Contributions to ^{1}H and ^{13}C Isotropic NMR Chemical Shielding Values (ppm) and NICS(1) values (ppm) for the Heterobenzenes (1−6)

	total			out-of-plane orbitals		
complexes	^{13}C	^{1}H	NICS(1)	O_π-^{13}C NMR	O_π-^{1}H NMR	O_π-NICS
(**1**)	−25.02	23.01	−14.98	−36.23	−0.47	−20.44
(**2**)	−34.78	22.98	−14.03	−36.21	−0.50	−18.57
(**3**)	−23.21	21.09	−11.60	−36.99	−0.92	−17.41
(**4**)	−30.02	21.12	−11.40	−34.61	−0.85	−18.23
(**5**)	−29.12	21.50	−11.54	−33.02	−0.74	−18.02
(**6**)	−30.12	20.23	−11.50	−34.04	−0.83	−17.61

considerably different from the π-only values. We note that the proton shielding for complex **1** is 23.0 ppm, which corresponds to a downfield chemical shift of 6.5 ppm, as we would expect for an aromatic proton; however, the O_π-NMR value of −0.47 is a direct measure of the downfield shift due to the aromatic ring current. We note for completeness that the ^{13}C NMR shielding values follow the same trend.

Since the point group of the heterobenzenes is a subgroup of the D_{6h} symmetry of benzene, the induced current density maps in molecules **1**−**6** can be also be explained using the benzene orbital excitation diagrams presented by Steiner and Fowler,[58] Of the three occupied π-orbitals in benzene, the $1e_{1g}$ contributes most of the diatropic ring current (aromaticity) since translational transitions from them to the LUMO are allowed, but the $1a_{2u}$ orbital contributes very little. In the heterobenzenes, the aromaticity will be due to transitions from the valence b_1 and a_2 electrons, particularly those corresponding to the e_{1g} in benzene. A similar analysis to that used on the heterobenzenes will now be extended to the metallabenzenes.

Ring Current Analyses of the Metallabenzenes

The main interest regarding the aromaticity of the metallabenzenes is how the metal−ligand (M−L) d_π−p_π interactions at the metal center affect the delocalization of π-electrons in the ligand ring. We have studied 21 complexes (**7**−**27**) that have been previously considered by other researchers using different approaches. These can be classified into three groups. The first group, complexes **7**−**13**, are 18 electron systems, and the second group, **14**−**21**, are 16 electron complexes; however, all of these complexes have seven similar occupied out-of-plane orbitals. A third group, **22**−**27**, consists of some platinum and palladium complexes, which will be considered separately.

Previous EDA analysis has suggested that all of the metallabenzenes in the first two groups of complexes are aromatic, and each complex has 10 π-electrons in the metallocyclic ring.[51] Although we have analyzed all 15 complexes in the first two groups, we shall only present a detailed analysis of $Ir(C_5H_5)(PH_3)_2Cl_2$ (**7**) and $Os(C_5H_5)(PH_3)_2Cl_2$ (**14**) since the other complexes in these groups follow the same conclusions. First, we shall consider the 18 electron complexes, taking iridabenzene (**7**) as the main example.

Aromaticity in Irida- and Rhodabenzenes

Iridabenzenes are often regarded as being aromatic. Although the complexes exhibit downfield proton chemical shifts between 7 and 13 ppm, perhaps the more direct evidence comes from energy decomposition analysis, which has shown that the conjugated complexes are thermodynamically more stable with respect to the linear unconjugated fragments.[51] However, this evidence may not be conclusive since complex **9** has been shown experimentally to easily undergo a cycloaddition reaction.[45]

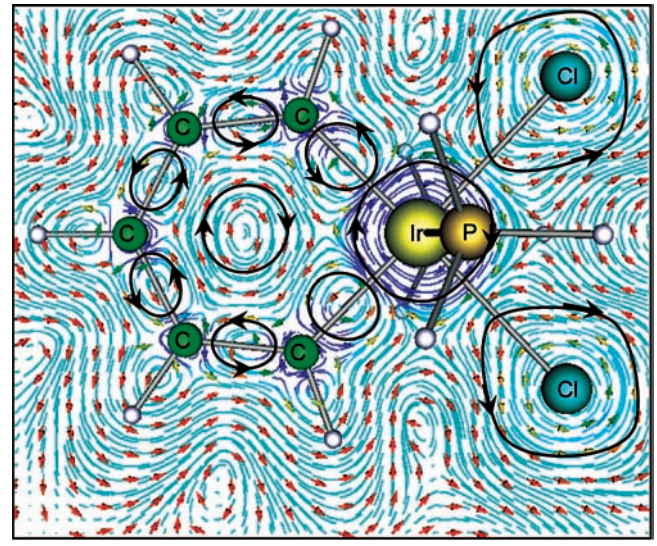

Figure 3. Total induced current density streamline plot for complex **7** in the ring plane.

As an example of the electronic structures of the iridabenzene (**7**−**10**) and the rhodabenzene (**11**−**13**) molecules, we have computed the induced current densities for $Ir(C_5H_5)(PH_3)_2Cl_2$ (**7**) in the plane of the ring (Figure 3) and at 1 bohr above the ring plane (Figure 4). The in-plane total current density plot clearly shows the local diatropic current around the metal atom as well as local currents corresponding to the C−C σ-bonds but no extensive delocalization. Moving onto the plots above the ring plane, where we might expect significant delocalization due to the π-bonding, Figure 4a−c shows a diatropic ring current around the ligand ring atoms, but it is clearly complicated and even disrupted by the inclusion of the metal core and σ- and nonbonding orbitals. A clearer picture emerges when we only consider the current density from the seven out-of-plane MOs rather than all MOs, and in Figures 4d−f, a diatropic current around the entire ring, including the metal, can now be seen. There is still some localized diatropic current at the metal due to electrons in the out-of-plane d_{xz} and d_{yz} orbitals, but this now forms part of the ring current and is of considerably smaller magnitude than the total metal diatropic current. Similar to the heterobenzenes, there is also a small paratropic current within the ligand ring; however, the outer diatropic current is slightly polarized away from the metal atom in the iridium complex. This is best illustrated in Figure 4e, where the contours show the magnitude of the out-of-plane induced current density and there are regions of maximum density lying just to the outside of the ring defined by a line joining the C−C and M−L bonds; in the heterobenzenes, the diatropic ring current was more directly over the nuclear centers. The ACID plots, Figure 4c and f, complement the current density plots, and the contours clearly show the extent of the electron delocalization in this system, even when all MOs are included. Other key features of the analysis are that there are strong local diatropic circulations at the metal center and at each chlorine atom. The magnetic fields classically arising from these induced currents, particularly due to the metal atom, will be significant contributors to the NICS and nuclear chemical shielding values and will later be shown to be largely responsible for the experimental downfield proton chemical shifts.

In order to understand the origin of the diatropic ring current in this case, we may consider the individual contributions from each molecular orbital. Complex **7**, which has C_{2v} point group symmetry, has seven out-of-plane (π-) molecular orbitals, of

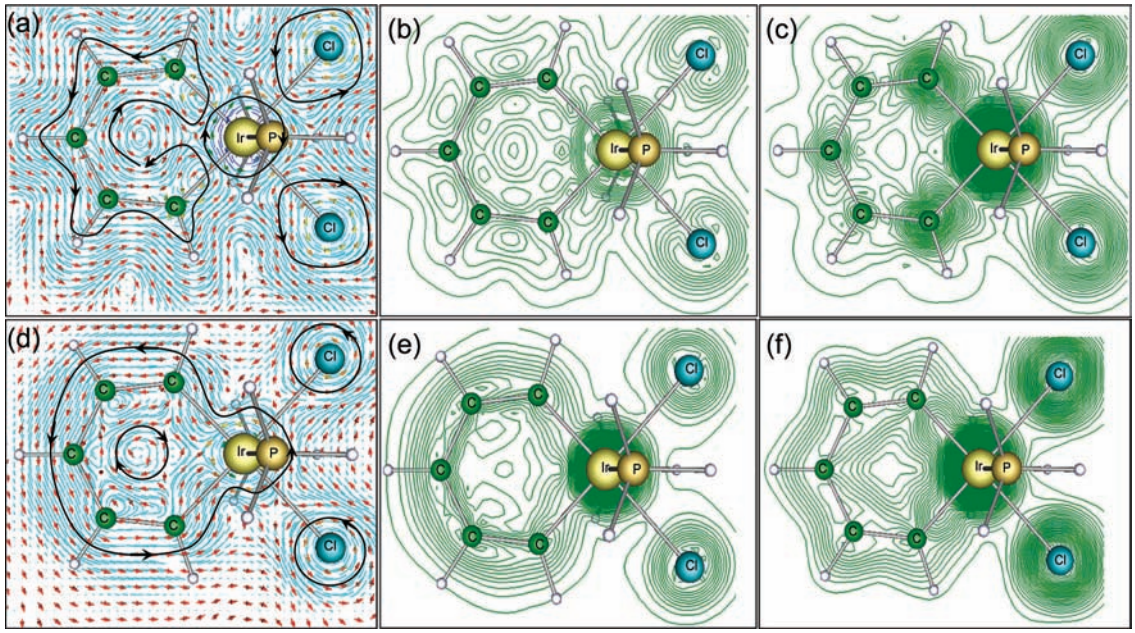

Figure 4. Induced current density and ACID plots for complex **7** at 1 bohr above the ring plane. The total induced current densities are shown (a) as a streamline plot, (b) with contours of the magnitude, and (c) with contours of the ACID values. Panels (d), (e), and (f) show the respective plots with the induced current densities due to out-of-plane MOs only.

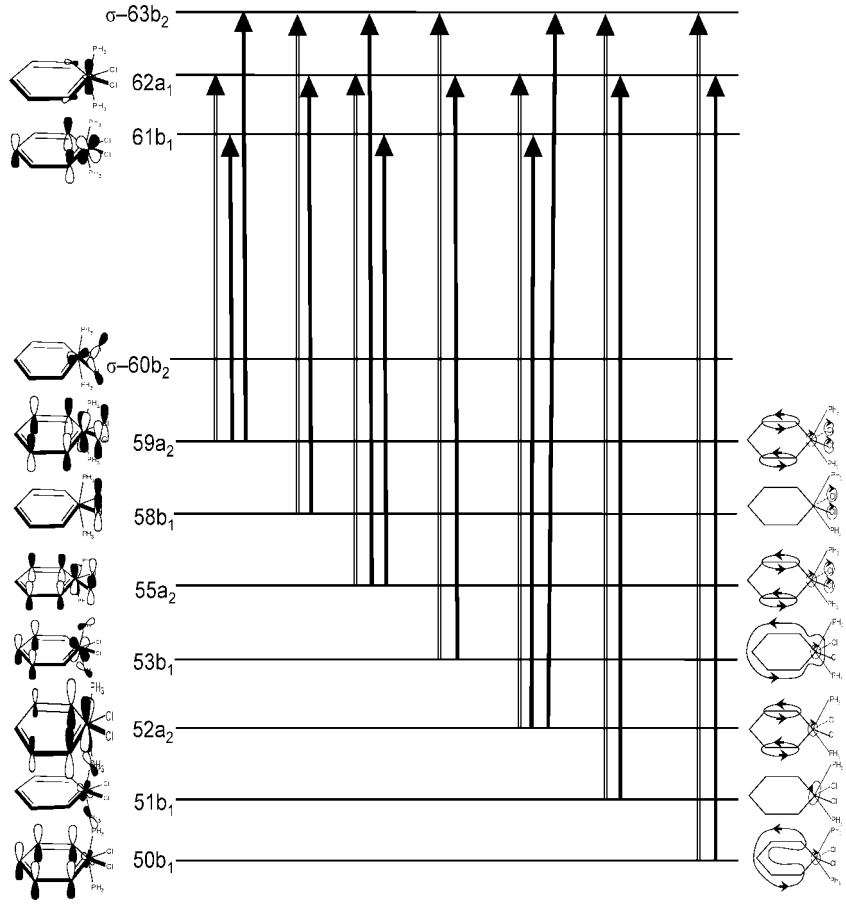

Figure 5. Molecular orbital diagram for complex **7**. The MOs are shown on the left-hand side, and schematic induced current density plots due to each MO are shown on the right. The bold filled vertical arrows correspond to allowed translational transitions, and the unfilled outline arrows correspond to rotational transitions.

which three are of a_2 symmetry and four are of b_1 symmetry. In Figure 5, a MO diagram is presented for complex **7**, including the out-of-plane and key valence in-plane orbitals. The allowed transitions that mainly give rise to diatropic ring currents (via the translational angular momentum operator, dark filled single arrows in Figure 5), are from a_2-occupied MOs to b_1- and b_2-unoccupied MOs and from b_1 to a_1 and a_2 MOs; the other allowed transitions, which we shall refer to as being paratropic (via the rotational operator, unfilled arrows in Figure 5), are from b_1 to b_2 and from a_2 to a_1. The induced current densities

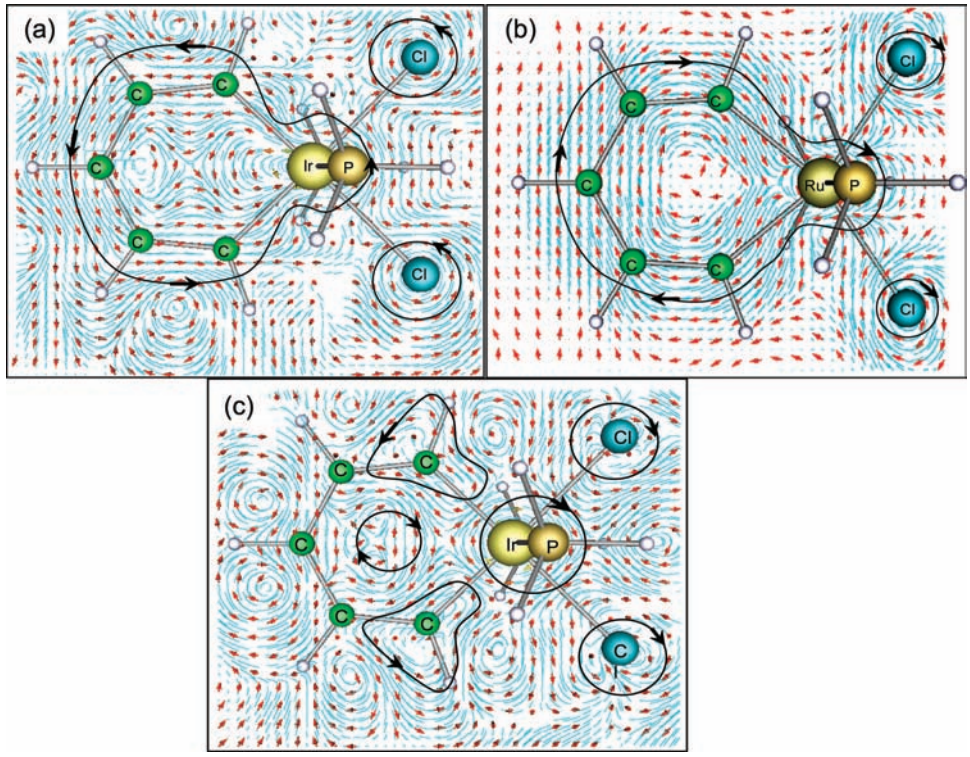

Figure 6. Orbital induced current density plots at 1 bohr above the ring plane for (a) the b_1 MOs of complex **7**, (b) the b_1 MOs of complex **14**, and (c) the a_2 MOs of complex **7**.

TABLE 2: Total Isotropic NICS(1) and Out-of-Plane O_π-NICS(1) Values for the Ir and Rh Benzenes (7−13) and the Total and Out-of-Plane-MO Isotropic NMR Chemical Shielding Values (ppm) of the Ring Protons[a]

	total chemical shielding				shielding due to out-of-plane orbitals			
complexes	$^1H_1$	$^1H_2$	$^1H_3$	NICS(1)	$^1H_1$	$^1H_2$	$^1H_3$	O_π-NICS(1)
(**7**)	20.01	21.11	24.02	−5.14 (−8.78)	−0.95	−0.50	−0.25	−8.23 (−26.50)
(**8**)	18.12	23.22	28.01	−9.70 (−4.43)	−1.51	−1.21	0.20	−2.82 (−9.76)
(**9**)	23.34	24.22	28.76	−3.21 (−6.86)	−0.65	−0.52	1.21	−3.49 (−10.12)
(**10**)	19.23	20.67	24.23	−8.97 (−7.37)	−0.78	−0.42	1.23	−4.31 (−12.23)
(**11**)	20.31	21.61	24.13	−4.14 (−9.23)	−0.67	−0.22	0.93	−8.23 (−25.28)
(**12**)	18.42	23.92	28.65	−7.70 (−4.98)	−1.34	−1.32	1.01	−2.82 (−9.87)
(**13**)	19.63	20.87	24.42	−5.97 (−7.35)	−0.59	−0.30	1.23	−4.31 (−12.34)

[a] The *zz* components, perpendicular to the ring plane, of the chemical shielding tensor ($NICS(1)_{zz}$ and O_π-$NICS(1)_{zz}$) are given in parentheses.

contributed by each MO are shown in the small schematic plots on the right-hand side of each energy level in Figure 5, and the total current density would be the sum of these individual MO contributions. It can be seen in Figure 6a that the contributions from the bonding b_1 orbitals are the main influence in creating an overall dominant diatropic ring current since the a_2 orbital involves antibonding M−L interactions and leads to localized and turbulent currents (see Figure 6c). To illustrate the relative importance of each individual MO to the total diatropic or paratropic current density, we prefer to compare the O-NICS(1) index for each orbital since we have found that interpretation of the relative magnitudes of the induced ring currents directly from the orbital plots can be somewhat ambiguous, although we note that the current density map for electrons in the $53b_1$ MO (Figure 5) is particularly similar to that observed for the combined out-of-plane electrons in Figure 4d.

The overall aromatic character of these complexes is more quantitatively suggested by the large negative O_π-NICS and proton O_π-NMR values (combining all of the out-of-plane orbital contributions) shown in Table 2. O-NICS(1) values corresponding to each MO are also listed in Table 3 and show that the

TABLE 3: O-NICS(1) Values (ppm) for the Out-of-Plane MOs of Complexes 7 and 14

MOs	O-NICS(1) complex (**7**)	complex (**14**)
59	−0.33	−5.28
58	0.02	0.33
55	−1.56	−4.99
53	−2.02	7.70
52	−1.02	−3.27
51	−2.10	4.07
50	−1.22	4.61

electrons in the $53b_1$ and $55b_1$ MOs contribute approximately −2 ppm per MO to the overall out-of-plane NICS(1) value, which itself is an indication of the magnitude of the diatropic ring current. The large contribution from MO $51b_1$ highlights the difficulty in unambiguously attributing NICS values directly to a diatropic ring current since the current is clearly localized on the metal atom. Similarly, it is clear that the complexity of the ring current is not easily described in terms of individual electrons, although considering both the schematic orbital current density plots in Figure 5 together with the O-NICS(1) values in Table 3 does imply that the $53b_1$ and $55b_1$ electrons may be

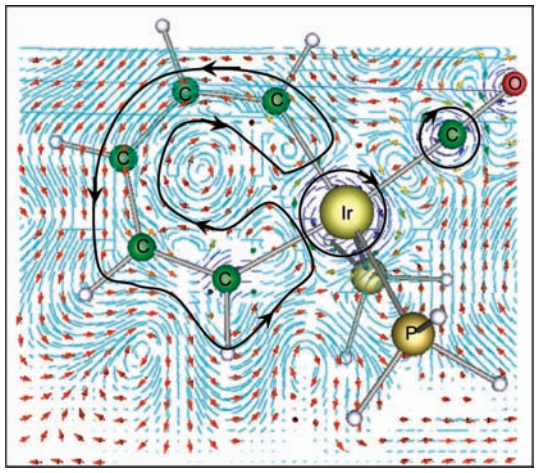

Figure 7. Induced current density plot for complex **8** at 1 bohr above the ring plane due to out-of-plane MO's only.

the most significant when describing the origin of the diatropic current. The most illuminating aspect of the O-NICS(1) analysis arises when we compare the values for complex **7** with those for complex **14**, which we shall discuss in the next section.

An important aspect of the analysis is that the O_π-NICS(1) values in Table 2 for complexes **7**−**13** do not follow the same trend as the NICS(1) indices, some being larger and others smaller. This is due to the large core and (in-plane) metal−ligand and ligand molecular orbital contributions, which are still significant at 1 a_0 above the plane in these complexes and which make the total isotropic NICS(1) index a particularly unreliable indicator of aromaticity for metal complexes. This can be further illustrated when we only consider the *zz* component, perpendicular to the ring, of the chemical shielding tensor. Both $NICS(1)_{zz}$ and O_π-$NICS(1)_{zz}$ values are also presented in Table 2 (in parentheses), and each clearly follows the same trend as the O_π-NICS(1) values, confirming the unreliability of the standard isotropic NICS(1) indices.

The ring currents for the other complexes, **8**−**13**, are very similar to those for complex **7**, although some distortion of the ring current is common; for example, the out-of-plane current density for complex **8**, shown in Figure 7, is now no longer symmetric. Complex **9** has generally higher O_π-NICS and O_π-NMR values than, for example, complex **7**, and thus, the nonaromatic nature of this complex is likely to be the reason for its more favorable cycloaddition reaction. Complex **10** is also clearly less aromatic than **7**, with a lower O_π-NICS value (see Table 2) in clear agreement with the EDA analyses. Although rhodium is in the same periodic group as iridium, the current density plots and NICS and NMR shielding values for the out-of-plane valence orbitals of complexes **11**−**13** (Table 2) are very similar to their iridium counterparts. This complements the findings of the EDA analysis; there is little difference in the aromaticity of the 4d and the 5d elements, and the stability difference between the two series might depend upon in-plane orbitals.[51]

The O_π-NMR values for the three ring protons, labeled H_1, H_2. and H_3 (for labeling, see Figure 1), are comparable with each other, and there is little variation between the values for the seven complexes. The shielding contribution due to the out-of-plane MOs is considerably smaller than the total NMR shift, indicating that the ring current for these systems is only a small contributor to the overall downfield shift, the main part of this shift arising from other MOs such as those localized at the metal center. For example, for complex **7**, we predict a downfield chemical shift for H_1 of 9 ppm, but the corresponding shielding contribution due to the out-of-plane orbitals is an order of magnitude smaller, −0.95 ppm (note: the negative sign of the shielding constant corresponds to a downfield shift). In addition, all of the complexes have negative O_π-NMR chemical shielding values for $^1H_1$ (ranging from −0.6 to −1.5 ppm), which are slightly more positive for $^1H_3$ (ranging from −0.3 to +1.2) due to the influence of the local diatropic circulation at the metal center; this difference is comparable with the experimental chemical shifts between these protons.

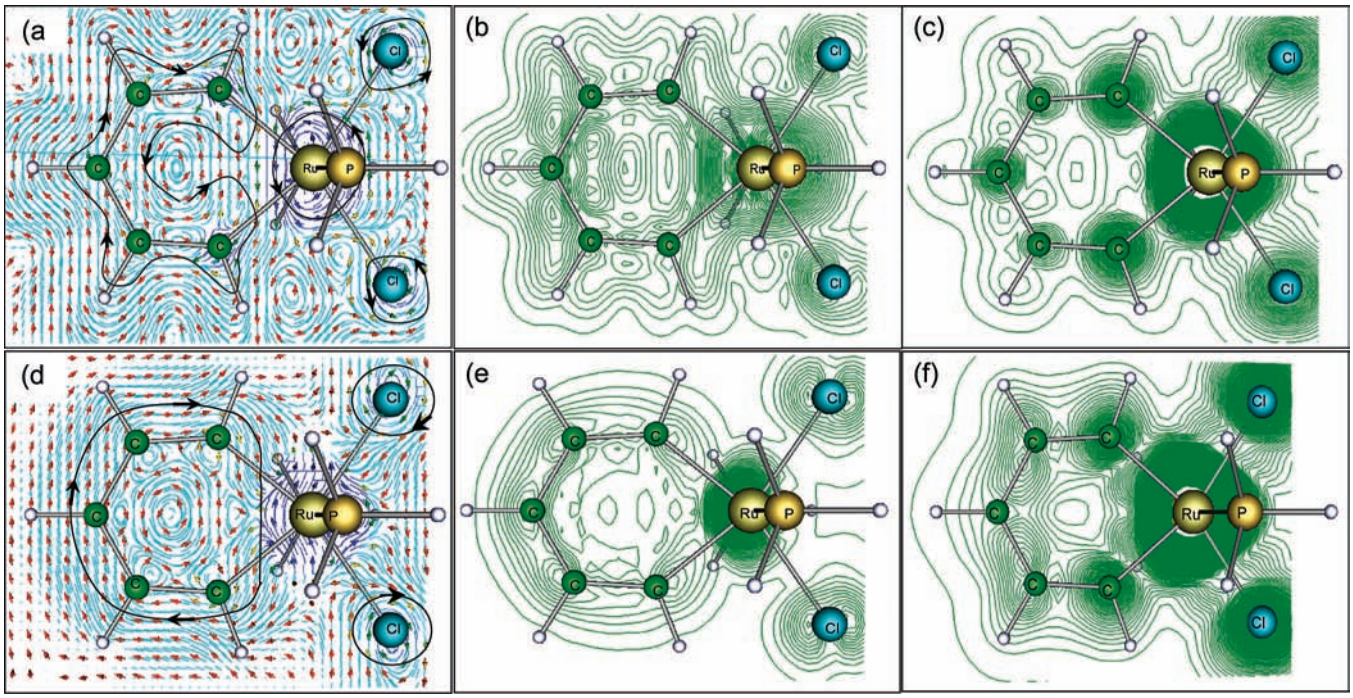

Figure 8. Induced current density and ACID plots for complex **14** at 1 bohr above the ring plane. The total induced current densities are shown (a) as a streamline plot, (b) with contours of the magnitude, and (c) with contours of the ACID values. Panels (d), (e), and (f) show the respective plots with the induced current densities due to out-of-plane MOs only.

TABLE 4: Total Isotropic NICS(1) and Out-of-Plane O_π-NICS(1) Values for the Os and Ru Benzenes (14−21) and the Total and Out-of-Plane-MO Isotropic NMR Chemical Shielding Values (ppm) of the Ring Protons[a]

	total chemical shielding				shielding due to out-of-plane orbitals			
complexes	$^1H_1$	$^1H_2$	$^1H_3$	NICS(1)	$^1H_1$	$^1H_2$	$^1H_3$	O_π-NICS(1)
(**14**)	15.25	20.67	16.54	14.39 (10.23)	−1.63	0.17	0.90	3.17 (10.93)
(**15**)	15.24	21.45	17.32	7.32 (7.27)	−1.70	1.31	0.51	2.68 (7.98)
(**16**)	16.23	23.24	20.01	3.91 (14.26)	−0.95	−0.01	1.05	8.08 (24.25)
(**17**)	13.23	21.25	17.67	2.67 (−6.01)	−1.44	−0.35	0.22	−1.12 (−4.76)
(**18**)	14.98	19.56	16.21	12.64 (5.76)	−0.95	1.13	3.05	1.62 (4.58)
(**19**)	13.67	20.54	16.21	7.40 (12.26)	−1.61	1.21	5.25	10.31 (29.72)
(**20**)	13.52	23.72	19.23	5.08 (8.25)	−2.52	0.26	1.64	8.95 (23.34)
(**21**)	16.25	22.52	19.52	3.71 (6.92)	−4.21	0.77	0.14	6.59 (18.15)

[a] The *zz* components, perpendicular to the ring plane, of the chemical shielding tensor ($NICS(1)_{zz}$ and O_π-$NICS(1)_{zz}$) are given in parentheses.

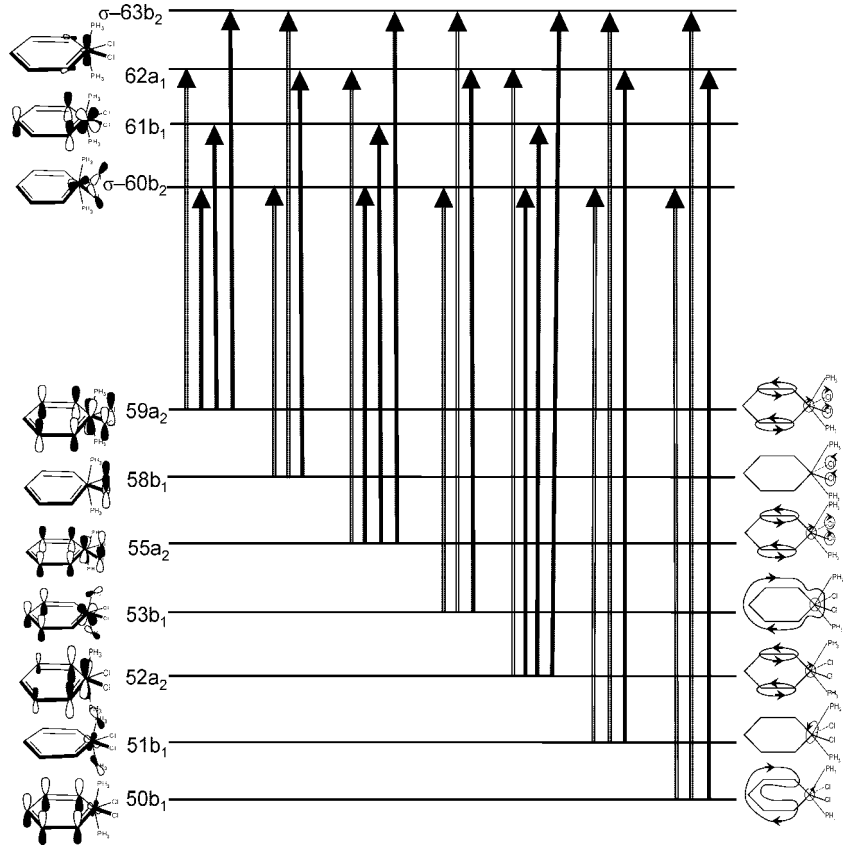

Figure 9. Molecular orbital diagram for complex **14**. The MOs are shown on the left-hand side, and schematic induced current density plots due to each MO are shown on the right. The bold filled vertical arrows correspond to allowed translational transitions, and the unfilled outline arrows correspond to rotational transitions.

Here, we should note that although the absolute shielding values between CSGT and GIAO methods can be considerably different, there is nevertheless very reasonable agreement between the relative values of the chemical shifts for the complexes with both the CSGT and GIAO methods and with respect to experiment. We should also point out that although larger basis sets may improve absolute agreement with experiment, these differences are relatively small and do not change any of the trends or conclusions.

Aromaticity in Osma- and Ruthenabenzenes

To contrast with the irida- and rhodabenzene complexes, we shall now consider eight 16 electron osmium and ruthenium complexes, **14**−**21**. As with the Ir and Rh complexes, downfield chemical shifts again strongly suggest that the Os and Ru benzenes are aromatic,[45] although energy decomposition analysis[51] indicates that they may be less aromatic than their 18 electron Ir and Rh counterparts. However, there is no evidence

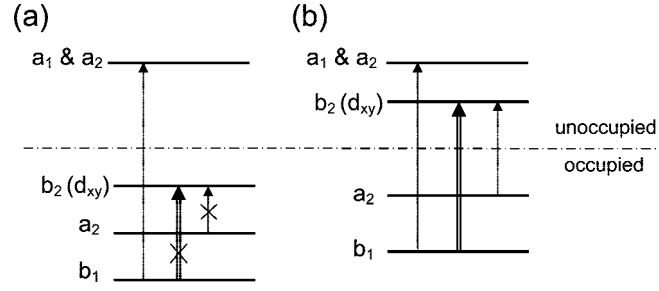

Figure 10. Schematic summarizing the difference in transitions contributing to the ring currents of (a) the 18e Ir and Rh benzenes and (b) the 16e Os and Ru benzenes. The single line vertical arrows correspond to translational transitions (diatropic current), and the double line arrows correspond to rotational transitions (paratropic current).

TABLE 5: Proton NMR Chemical Shifts (ppm) for the Ring Protons of the Ir, Rh, Os, and Rh Benzenes and Pd and Pt Complexes Computed with the CSGT and GIAO Methods[a,b]

	CSGT			GIAO		
complexes	$^1H_1$	$^1H_2$	$^1H_3$	$^1H_1$	$^1H_2$	$^1H_3$
(**7**)	9.46	8.36	5.45	11.32	8.52	6.90
	13.95[c]	−	*7.86*[c]			
(**8**)	11.35	5.25	*2.46*	12.98	6.98	6.85
	11.26[c]	−	*7.37*[c]			
(**9**)	11.15	5.26	1.72	12.26	6.98	5.25
	13.02[c]	−	*8.16*[c]			
(**10**)	10.24	8.80	5.24	11.23	8.84	6.75
	12.61	*6.79*	*7.15*			
(**11**)	9.16	7.87	5.34	12.97	7.90	7.09
(**12**)	11.05	5.55	1.02	11.30	6.84	6.87
(**13**)	9.85	8.61	5.05	10.10	8.81	6.78
(**14**)	14.22	12.93	8.80	12.25	9.32	6.60
	12.74	*6.96*	*6.40*			
(**15**)	14.24	12.15	8.02	12.58	7.98	7.79
(**16**)	13.24	9.47	6.23	12.81	7.23	7.07
	12.61	*7.15*	*6.79*			
(**17**)	16.24	11.80	8.22	13.95	6.68	6.42
	13.27	*7.07*	*6.61*			
(**18**)	14.49	13.26	9.91	13.65	9.57	10.83
(**19**)	15.80	13.26	8.93	12.33	8.21	7.91
(**20**)	15.95	10.24	5.75	13.60	7.47	7.22
(**21**)	13.23	9.95	6.95	11.78	6.94	6.59
(**22**)	12.98	3.24	5.24	11.45	6.52	6.25
(**23**)	9.78	8.22	5.13	9.53	6.54	7.24
(**24**)	9.95	9.38	6.35	11.28	7.12	7.72
(**25**)	7.95	5.24	3.46	10.13	7.09	7.91
(**26**)	10.95	8.22	5.24	10.46	6.65	7.57
(**27**)	10.91	7.24	4.95	10.22	6.56	7.28

[a] Chemical shifts are with respect to TMS; isotropic chemical shielding values for TMS are 29.47 and 31.75 at the CSGT and GIAO levels, respectively. [b] Experimental chemical shift values[44] (ppm) are shown in italics. [c] H at C_2 replaced by the ^{i}Pr group.

for cycloadition reactions in the Os and Ru benzenes, which suggests that the electronic natures of these complexes are completely different from **7** to **13** and that the reactivity difference is due to the σ-bonds and not due to the π-bonds.[51]

In Figure 8 we have computed total (a−c) and out-of-plane (d−f) induced current densities for complex **14** at 1 bohr above the plane. For this complex, typical of complexes **15**−**21**, there is a strong paratropic (clockwise) circulation around the ring in contrast to that for complexes **7**−**13** shown in Figure 4. In the total density plots, the ring current is disrupted between the C−C and M−C bonds, and there is a diatropic circulation at the metal and chlorine centers. The general lack of electron delocalization in these molecules is particularly evident in the ACID plots using either the total or the out-of-plane current density (Figure 8c and f, respectively). When the current density for only the seven out-of-plane molecular orbitals is considered (Figure 8d and e), there is an overall paratropic circulation which is characteristic of the antiaromatic nature of a molecule.

The strong paratropic circulation is also quantitatively reflected by the positive O_π-NICS and O_π-NMR shielding values (Table 4), which are in contrast to negative values for the Ir and Rh complexes. This difference can be explained using the molecular orbital diagram, Figure 9. The principle difference between the Ir and Os complexes is that although both have the same valence MOs, in the Ir complexes, the HOMO is an in-plane $M-Cl_2$ antibonding orbital, and in the Os complexes, this orbital ($60b_2$) is now the LUMO. Although, in the Ir complexes, there were no allowed transitions to or from this orbital, in the Os complexes such as complex **14**, there are transitions allowed to it from the occupied b_1 orbitals; these additional rotational transitions result in significant disruption of the ring current. In Table 3, O-NICS(1) values for each MO of complexes **7** and **14** are compared. If we consider the changes in these values due to the absence of the two in-plane electrons (from the $60b_2$ MO) of the 16 electron system, for $52a_2$, $55a_2$, and $59a_2$, the O-NICS values are more negative for **14** than those for **7** (ΔNICS(**7**→**14**) = −2.3, −3.4, and −5.0 ppm, respectively) mainly due to the a_2 to $60b_2$ translational transitions, which are now allowed; the negative change indicates an increase in the diatropic character of the ring current. However, for the $50b_1$, $51b_1$, and $53b_1$ MOs, the O-NICS values are more positive (by 5.8, 6.2, and 9.7 ppm, respectively), mainly due to the b_1 to $60b_2$ rotational transitions, changing the overall ring current into a clearly paratropic one. These conclusions are summarized in Figure 10. In the 18e Ir and Ru benzenes (**7**−**13**), transitions from the out-of-plane b_1 and a_2 to the in-plane b_2 HOMO are formally forbidden since they are all occupied; however, in the 16e Os and Ru benzenes (**14**−**21**), significant paratropic transitions are now allowed since the b_2 MO is now unoccupied. In each case, the b_2 MO has considerable (over 50%) metal d_{xy} (in-plane) character. Although it is not possible to quantify these transitions exactly, the difference between the O_π-NICS values of **7** and **14,** +11 ppm, can be partitioned between a paratropic contribution arising from transitions to the $60b_2$ LUMO from the b_1 orbitals of +22 ppm, negated to some extent by a diatropic contribution due to transitions from the a_2 orbitals of −11 ppm. This change from a diatropic to paratropic ring current can be visualized by comparing the current density arising from the b_1 electrons of **7** in Figure 6a with that from the b_1 electrons of **14** shown in Figure 6b, each current map being very similar to the corresponding maps for MO $53b_1$.

Similar to complex **7**, the experimental downfield proton chemical shifts in **14** are due to the electrons localized at the metal center, as shown in both the total and O_π-NMR chemical shift difference between H_1 (∼12 ppm) and H_3 (6−7 ppm) in the same ring (see Table 4). Overall, we conclude that it is the presence of the extra two in-plane electrons of the 18 electron system which moves the ring proton chemical shielding constants downfield relative to the 16 electron system.

If we now consider the other complexes, **15**−**21**, and compare each with its Ir or Rh 18e counterpart, each shows a similar change from a diatropic to a paratropic ring current. The O_π-NICS and O_π-NMR shielding values (Table 2) suggest that as the coordination environment at the metal center in these molecules is changed, there is a change in antiaromatic character.

Similar to the Ir and Rh benzenes (**7**−**13**), we believe that the NICS(1) index is somewhat more unreliable than the O_π-NICS(1) values as an indicator of aromaticity in the Os and Ru complexes. Again, the $NICS(1)_{zz}$ and O_π-$NICS_{zz}$ values for these complexes (shown in Table 4 in parentheses) follow the same trend as the O_π-NICS(1) values, in contrast to the variation of the isotropic NICS(1) indices. From the O_π-NICS(1) values, we may conclude that antiaromatic character decreases in the following order for the osmabenzenes, (**16**) > (**14**) > (**15**) > (**17**), and for ruthenabenzenes, (**19**) > (**20**) > (**21**) > (**18**).

Aromaticity in Platina- and Palladabenzenes

A range of Pd and Pt cyclopentadienyl complexes, **22**−**27**, have recently been synthesized.[45] Chemical shifts for these molecules have been computed at the CSGT and GIAO levels and are summarized in Table 5. The chemical shifts for all of the complexes were found to be significantly downfield, with values ranging from 3.2 to 16.0 ppm.

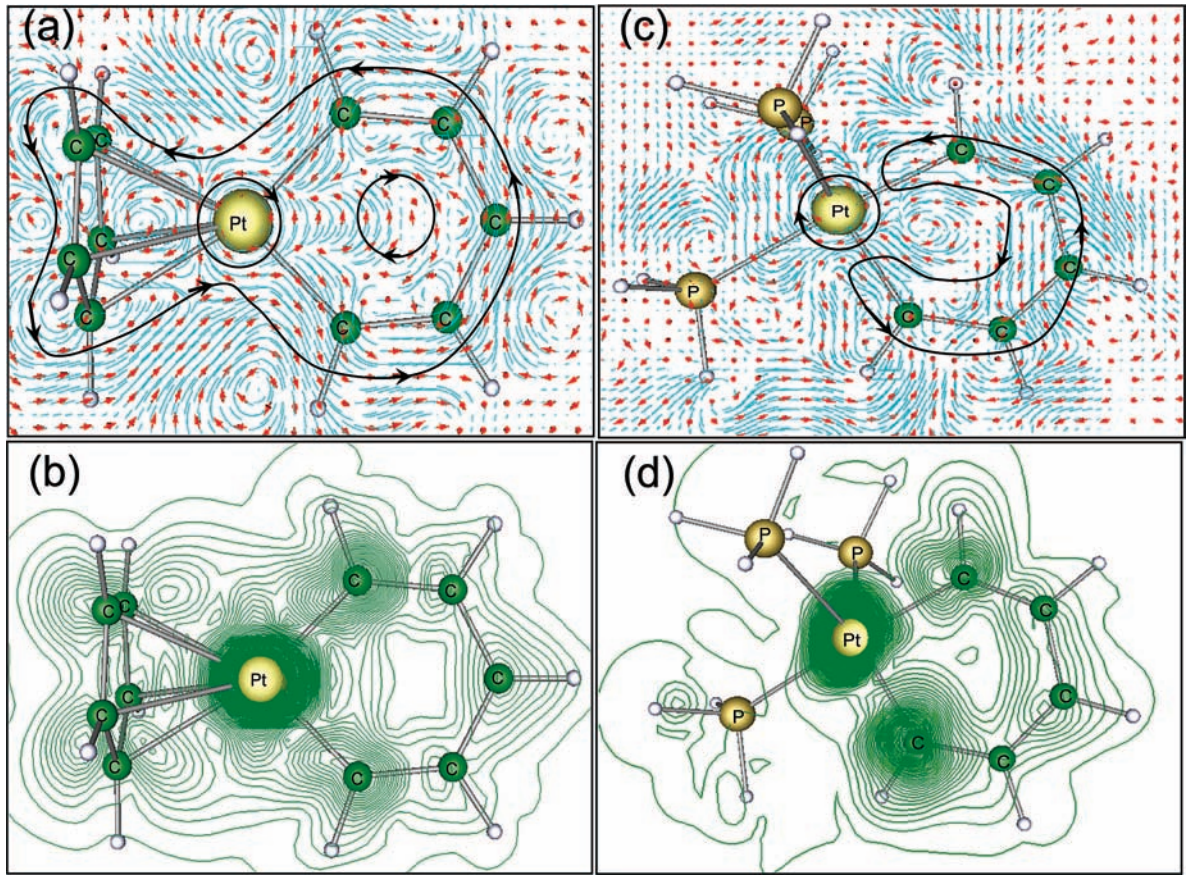

Figure 11. Induced current density of complexes (a) **22** and (c) **24** and ACID plots for (b) **22** and (d) **24** for the out-of-plane MOs at 1 bohr above the ring plane.

TABLE 6: Total NICS(1) and Out-of-Plane O_π-NICS(1) Values for the Pd and Pt Complexes (22−27) and the Total and Out-of-Plane-MO Isotropic NMR Chemical Shielding Values (ppm) of the Ring Protons

	total chemical shielding				shielding due to out of plane orbitals			
complexes	$^1H_1$	$^1H_2$	$^1H_3$	NICS(1)	$^1H_1$	$^1H_2$	$^1H_3$	O_π-NICS(1)
(**22**)	21.49	24.23	26.23	−21.82	−0.32	−0.33	−0.14	−5.75
(**23**)	20.69	24.34	21.25	12.62	2.60	2.32	1.73	2.22
(**24**)	19.52	23.12	20.09	−6.20	−0.48	−0.39	1.04	0.02
(**25**)	21.52	26.01	24.23	−21.08	−0.39	−0.33	−0.25	−7.27
(**26**)	18.52	24.23	21.25	6.23	0.21	0.61	1.51	2.74
(**27**)	18.56	24.52	22.23	−5.10	−0.46	−0.29	1.04	0.02

Let us consider the cyclopentadienyl complexes, **22**, and the phosphine complex, **24**, for platinum first. The out-of-plane induced current densities for the five valence out-of-plane MOs at 1 bohr above the benzyl ring have been computed and are presented in Figure 11. In the current density and ACID plot for complex **22** (Figure 11a and b), there is a diatropic current which encompasses the entire molecule including the cyclopentadienyl ligand. The corresponding O_π-NICS(1) and O_π-NMR proton chemical shielding (Table 6) all support the conclusion and the previous study of the ACID of this molecule,[40] that there is significant aromatic character in this complex and that it may be more aromatic than the hetero benzenes. In contrast, when the cyclopentadiene ring is replaced by electron-donating PH_3 ligands, for example, in complex **24** (Figure 11c and d), there significant distortion of the diatropic current to such an extent as to disrupt the aromaticity entirely, and delocalization of the out-of-plane electrons is limited to the C_5H_5 ligand. The same trend is observed with both PH_3 complexes (**23** and **24**) and with the respective Pd complexes (**26** and **27**). The resulting nonaromatic character of these phosphine complexes is reflected in their positive O_π-NICS and O_π-NMR values (Table 6).

Conclusions

The analyses of the electronic structure of a range of metallabenzenes has shown that the isotropic NMR chemical shift values for ring protons do not provide reliable evidence of aromaticity. The induced current corresponding to the out-of-plane MOs in the metallabenzene six-membered ring of all of the 18 electron complexes, **8**−**13** (see Figure 1) is diatropic in each case; however, the ring current is paratropic for each of the 16 electron complexes, **14**−**21**. The downfield NMR chemical shifts are mainly due to the strong local diatropic currents at the metal and other nuclear centers, with only a small contribution from the ring π-electrons in the case of complexes **8**−**13**. In complexes **14**−**21**, the contribution from the metallocycle π-electrons is, in fact, upfield. Although the other ligands do not affect these observations overall, they do have subtle effects on the magnitude of the ring current, and these differences have been quantified by O_π-NICS and O_π-NMR

shielding values; by removing the strong diatropic contributions of the core and in-plane metal and ligand orbitals, we have shown that isotropic NICS and NMR shielding values can be a reliable indication of the degree of delocalization of the electrons for these systems, although isotropic experimental and theoretical values which include all electrons, for example, NICS(1), can be easily misinterpreted.

In conclusion, we have shown that the 18 electron Ir and Rh metallabenzene complexes studied in this paper all exhibit diatropic ring currents and magnetic shielding properties consistent with aromaticity, where as the 16 electron Os and Ru complexes all show ring currents typical of antiaromatic character despite having the same occupancy of π-MOs. The differences can be directly attributed to the HOMO/LUMO b_2 in-plane (d_{xy}) molecular orbital, which, when unoccupied, allows mixing that leads to disruption of the delocalization typical of aromatic systems. We have also shown that the platinum and palladium metallabenzenes are highly aromatic when coordinated to the cyclopentadienyl ligand alone (**22** and **25**). For both metals, when the cyclopentadienyl ligand is replaced by $(PH_3)_2$ or $(PH_3)_3$, (**23**, **24**, **26**, **27**), the complex becomes nonaromatic.

Acknowledgment. We would like to thank The University of Manchester and Universities UK for ORS studentship funding and the NWDA and NWGrid consortium for computational resources. We would like to also acknowledge Prof. P. Fowler for invaluable advice during in the early stages of the research and Prof. G. Frenking for a preprint of the EDA analysis results.

References and Notes

(1) (a) Lazzeretti, P. *Prog. Nucl. Magn. Reson. Spectrosc.* **2000**, *36*, 1. (b) Gomes, J. A. N. F.; Mallion, R. B. *Chem. Rev.* **2001**, *101*, 1349.
(2) Schleyer, P. v. R.; Jiao, H.; Maerker, C.; Dransfeld, A.; Jiao, H.; Eikema Hommes, N. J. R. *J. Am. Chem. Soc.* **1996**, *118*, 6317.
(3) (a) Boldyrev, A. I.; Wang, L.-S. *Chem. Rev.* **2005**, *105*, 3716. (b) Masui, H. *Coord. Chem. Rev.* **2001**, *219*, 957.
(4) Pauling, L. *J. Chem. Phys.* **1936**, *4*, 673.
(5) Lonsdale, K. *Proc. R. Soc. London, Ser. A* **1937**, *159*, 149.
(6) (a) London, F. *C.R. Acad. Sci. (Paris)* **1937**, *28*, 205. (b) London, F. *J. Chem. Phys.* **1937**, *5*, 837.
(7) Sondheimer, F. *Proc. R. Soc. London, Ser. A* **1967**, *297*, 173.
(8) Katritzky, A. R.; Karelson, M.; Wells, A. P. *J. Org. Chem.* **1996**, *61*, 1619.
(9) Pople, J. A. *J. Chem. Phys.* **1964**, *41*, 2559.
(10) Ferguson, A. F.; Pople, J. A. *J. Chem. Phys.* **1965**, *42*, 1560.
(11) Coulson, C. A.; Mallion, R. B. *J. Am. Chem. Soc.* **1976**, *98*, 592.
(12) Laali, K. K.; Bolvig, S.; Raeker, T. J.; Mitchell, R. H. *J. Chem. Soc., Perkin Trans. 2* **1996**, *12*, 2635.
(13) Cook, M. J.; Katritzky, A. R.; Linda, P. *Adv. Heterocycl. Chem.* **1974**, *17*, 255.
(14) Lewis, D.; Peters, D. *Facts and Theories of Aromaticity*; Macmillan: New York, 1975.
(15) Balaban, A. T. *Chemical Applications of Graph Theory*; Academic Press: London, New York, and San Francisco, 1976.
(16) Graovac, A.; Gutman, I.; Trinajstic, N. *Topological Approach to the Chemistry of Conjugated Molecules*; Springer-Verlag: Berlin, Germany, 1977.
(17) Perlstein, J. H. *Angew. Chem., Int. Ed. Engl.* **1977**, *16*, 519.
(18) (a) Aihara, J.-I. *The Theory of Aromatic Stabilization: A Source Book 1974−1979*; Department of Chemistry, Faculty of Science, Hokkaido University: Japan, 1979.
(19) (a) Graovac, A., Trinajstic, N., International Symposium on Aromaticity, Dubrovnik, Croatia, Yugoslavia, Sept 3−5, 1979. (b) Agranat, I.; Hess, B. A., Jr.; Schaad, L. J. *Pure Appl. Chem.* **1980**, *52*, 1399.
(20) Balaban, A. T. *Pure Appl. Chem.* **1980**, *52*, 1409.
(21) Aihara, J. *J. Am. Chem. Soc.* **1981**, *103*, 5704.
(22) Lloyd, D. M. G. *Nonbenzenoid Conjugated Carbocyclic Compounds*; Elsevier: Amsterdam, The Netherlands, 1984.
(23) Garratt, P. J., *Aromaticity*; Wiley: New York, 1986.
(24) Wolinski, K.; Hinton, J. F.; Pulay, P. *J. Am. Chem. Soc.* **1990**, *112*, 8251.
(25) Keith, T. A.; Bader, R. F. W. *Chem. Phys. Lett.* **1993**, *210*, 223.
(26) Pople, J. A. *Mol. Phys.* **1958**, *1*, 175.
(27) McWeeny, R. *Mol. Phys.* **1958**, *1*, 311.
(28) Waugh, J. S.; Fessenden, R. W. *J. Am. Chem. Soc.* **1957**, *79*, 846.
(29) Waugh, J. S.; Fessenden, R. W. *J. Am. Chem. Soc.* **1958**, *80*, 6697.
(30) Johnson, C. E.; Bovey, F. A. *J. Chem. Phys.* **1958**, *29*, 1012.
(31) Dailey, B. P. *J. Chem. Phys.* **1964**, *41*, 2304.
(32) Karplus, M.; Pople, J. A. *J. Chem. Phys.* **1963**, *38*, 2803.
(33) (a) Long, E. R.; Memory, J. D. *J. Chem. Phys.* **1976**, *65*, 2918. (b) van Vleck, J. H. *The Theory of Electric and Magnetic Susceptibilities*; Oxford University Press: Oxford, U.K., 1932.
(34) Ramsey, N. F. *Phys. Rev.* **1950**, *78*, 699.
(35) Ramsey, N. F. *Phys. Rev.* **1952**, *86*, 243.
(36) Steiner, E.; Fowler, P. W. *J. Phys. Chem. A* **2001**, *105*, 9553.
(37) Steiner, E.; Fowler., P. W. *Chem. Commun.* **2001**, *21*, 2220.
(38) (a) Zanasi, R.; Fowler, P. W. *Chem. Phys. Lett.* **1995**, *238*, 270. (b) Fowler, P. W.; Zanasi, R.; Cadioli, B.; Steiner, E. *Chem. Phys. Lett.* **1996**, *251*, 132.
(39) Heine, T.; Schleyer, P. v. R.; Corminboeuf, A.; Seifert, G.; Reviakine, R.; Weber, J. *J. Phys. Chem. A* **2003**, *107*, 6470.
(40) Geuenich, D.; Hess, K.; Kohler, F.; Herges, R. *Chem. Rev.* **2005**, *105*, 3758.
(41) (a) Wannere, C. S.; Corminboeuf, C.; Allen, W. D.; Schaefer, H. F.; Schleyer, P. v. R. *Org. Lett.* **2005**, *7*, 1457. (b) Faglioni, F.; Ligabue, A.; Pelloni, S.; Soncini, A.; Viglione, R. G.; Ferraro, M. B.; Zanasi, R.; Lazzeretti, P. *Org. Lett.* **2005**, *7*, 3457. (c) Osuna, S.; Poater, J.; Bofill, J. M.; Alemany, P.; Sola, M. *Chem. Phys. Lett.* **2006**, *428*, 191.
(42) (a) Makedonas, C.; Mitsopoulou, C. A. *Eur. J. Inorg. Chem.* **2006**, *12*, 2460. (b) Milcic, M. K.; Ostojic, B. D.; Zaric, S. D. *Inorg. Chem.* **2007**, *46*, 7109.
(43) Schleyer, P. v. R.; Puhlhofer, F. *Org. Lett.* **2002**, *4*, 2873.
(44) Doering, W. v. E.; Detert, L. *J. Am. Chem. Soc.* **1951**, *73*, 876.
(45) (a) Bleeke, J. E. *Chem. Rev.* **2001**, *101*, 1205. (b) He, G.; Xia, H.; Jia, G. *Chin. Sci. Bull.* **1004**, *49*, 1543.
(46) Mitchell, R. H. *Chem. Rev.* **2001**, *101*, 1301.
(47) Rickard, C. E. F.; Roper, W. R.; Woodgate, S. D.; Wright, L. J. *Angew. Chem., Int. Ed.* **2000**, *39*, 750.
(48) (a) Chamizo, J. A.; Morgoda, J.; Sosa, P. *Organometallics* **1993**, *12*, 5005. (b) Pauling, L. *J. Chem. Phys.* **1936**, *4*, 673.
(49) Iron, M. A.; Lucassen, A. C. B.; Cohen, H.; van der Boom, M. E.; Martin, J. M. L. *J. Am. Chem. Soc.* **2004**, *126*, 11699.
(50) (a) Chen, Z.; Wannere, C. S.; Corminboeuf, C.; Ruchta, R.; Schleyer, P. v. R. *Chem. Rev.* **2005**, *105*, 3842. (b) De Proft, F.; Geerlings, P. *Phys. Chem. Chem. Phys.* **2004**, *6*, 242. (c) Schleyer, P. v. R.; Jiao, H.; Hommes, N. J. R. v. E.; Malkin, V. G.; Malkiria, O. L. *J. Am. Chem. Soc.* **1997**, *119*, 12669.
(51) Fernandez, I.; Frenking, G. *Chem.—Eur. J.* **2007**, *13*, 5873.
(52) Bader, R. F. W.; Anderson, S. G.; Duke, A. J. *J. Am. Chem. Soc.* **1979**, *101*, 1389.
(53) Steiner, E.; Fowler, P. W. *Phys. Chem. Chem. Phys.* **2004**, *6*, 261.
(54) Fallah-Bagher-Shaidaei, H.; Wannere, C. S.; Corminboeuf, C.; Puchta, R.; Schleyer, P. v. R. *Org. Lett.* **2006**, *8*, 863.
(55) (a) Becke, A. D. *J. Chem. Phys.* **1993**, *98*, 5648. (b) Lee, C.; Yang, W.; Parr, R. G. *Phys. Rev. B* **1988**, *37*, 785. (c) Miehlich, B.; Savin, A.; Stoll, H.; Preuss, H. *Chem. Phys. Lett.* **1989**, *157*, 200.
(56) (a) Hay, P. J.; Wadt, W. R. *J. Chem. Phys.* **1985**, *82*, 270. (b) Wadt, W. R.; Hay, P. J. *J. Chem. Phys.* **1985**, *82*, 284. (c) Hay, P. J.; Wadt, W. R. *J. Chem. Phys.* **1985**, *82*, 299.
(57) Frisch, M. J. Trucks, G. W.; Schlegel, H. B.; Scuseria, G. E.; Robb, M. A.; Cheeseman, J. R.; Montgomery, J. A.; Vreven, T., Jr.; Kudin, K. N.; Burant, J. C.; Millam, J. M.; Iyengar, S. S.; Tomasi, J.; Barone, V.; Mennucci, B.; Cossi, M.; Scalmani, G.; Rega, N.; Petersson, G. A.; Nakatsuji, H.; Hada, M.; Ehara, M.; Toyota, K.; Fukuda, R.; Hasegawa, J.; Ishida, M.; Nakajima, T.; Honda, Y.; Kitao, O.; Nakai, H.; Klene, M.; Li, X.; Knox, J. E.; Hratchian, H. P.; Cross, J. B.; Bakken, V.; Adamo, C.; Jaramillo, J.; Gomperts, R.; Stratmann, R. E.; Yazyev, O.; Austin, A. J.; Cammi, R.; Pomelli, C.; Ochterski, J. W.; Ayala, P. Y.; Morokuma, K.; Voth, G. A.; Salvador, P.; Dannenberg, J. J.; Zakrzewski, V. G.; Dapprich, S.; Daniels, A. D.; Strain, M. C.; Farkas, O.; Malick, D. K.; Rabuck, A. D.; Raghavachari, K.; Foresman, J. B.; Ortiz, J. V.; Cui, Q.; Baboul, A. G.; Clifford, S.; Cioslowski, J.; Stefanov, B. B.; Liu, G.; Liashenko, A.; Piskorz, P.; Komaromi, I.; Martin, R. L.; Fox, D. J.; Keith, T.; Al-Laham, M. A.; Peng, C. Y.; Nanayakkara, A.; Challacombe, M.; Gill, P. M. W.; Johnson, B.; Chen, W.; Wong, M. W.; Gonzalez, C.; Pople, J. A. *Gaussian 03*, revision C.02; Gaussian, Inc.: Wallingford, CT, 2004.
(58) Steiner, E.; Fowler, P. W.; Havenith, R. W. A. *J. Phys. Chem. A* **2002**, *106*, 7048.
(59) The CCP1 GUI Project. http://www.cse.scitech.ac.uk/ccg/software/ccp1gui/ (2008).

JP7106044